Journal of Luminescence 192 (2017) 599–607

Contents lists available at ScienceDirect

Journal of Luminescence

journal homepage: www.elsevier.com/locate/jlumin

Luminescent properties of Pr^{3+}-doped $SrZrO_3$ phosphors

T.J. Pérez-Juache[a], R. López-Juárez[b], E. Barrera-Calva[a], F. González[a,*]

[a] Departamento de Ingeniería de Procesos e Hidráulica, Universidad Autónoma Metropolitana-Iztapalapa, A.P. 55-534, 09340, Ciudad de México, Mexico
[b] Unidad Morelia del Instituto de Investigaciones en Materiales, Universidad Nacional Autónoma de México, Antigua Carretera a Pátzcuaro No. 8701, Col. Ex Hacienda de San José de la Huerta, C.P. 58190 Morelia, Michoacán, Mexico

ARTICLE INFO

Keywords:
Pr^{3+}
Pechini method
Solid-state method
Charge transfer band

ABSTRACT

In this work $Sr_{1-1.5x}Pr_xZrO_3$ phosphors with different Pr^{3+} contents were synthesized by polymerizable complex and high-temperature solid-state methods. The samples were calcined between 700–1400 °C. The crystal structure, microstructure and photoluminescence properties of the prepared powders were investigated by X-ray diffraction (XRD), scanning electron microscopy (SEM) and photoluminescence spectroscopy, respectively.

The relationship between luminescent properties and the different sintering temperatures was studied. It was found that calcination at high temperature may remarkably increase the luminescence for samples synthesized by both methods. Emission spectra for all samples show dominant bands ascribed to transitions from the $^3P_{0,1}$ energy levels to lower levels, particularly that one in the greenish-blue region, corresponding to the $^3P_0 \rightarrow {}^3H_4$ transition. However, the bands ascribed to the $^3P_{0,1} \rightarrow {}^{2S+1}L_J$ transitions corresponding to the red spectral region are not inhibited at all, in contrast to recent reports. The samples prepared by solid state method exhibit a charge transfer band (CTB) due to the presence of Ti^{4+} impurities.

1. Introduction

The understanding of processes that allow a better use of the solar spectrum is of crucial importance [1]. Producing materials with low impact on the environment is also part of the integral solutions that must be addressed to stop the deterioration of the terrestrial ecosystem. In recent years, luminescent materials, which can convert a broad spectrum of light into photons of a desired wavelength, have been proposed to minimize the losses in the solar-cell-based energy conversion process. Trivalent lanthanide ions are the prime candidates to achieve efficient spectral conversion because of their rich energy-level structure, known as the Dieke diagram that allows for facile photon management [2]. Among trivalent lanthanides, Pr^{3+} could play the role of the donor for spectral conversion of visible into near infrared (NIR) photons as long as its luminescent response in a host favors the $^3P_0 \rightarrow {}^3H_4$ transition, which possess enough energy to produce more than one photon in the NIR.

The photoluminescence (PL) and long after-glow (LAG) properties of some rare-earth-doped perovskite-type oxides with a chemical formula ABO_3 have been studied intensively. In these reports, it has been found that although orthorhombic perovskites are characterized by very similar structural features, they show different luminescence properties when doped with Pr^{3+}. In particular, Pr^{3+} doped $CaZrO_3$ and $CaTiO_3$ have been studied [3–5], and it was found that Pr^{3+} in $CaZrO_3$ exhibits the typical greenish-blue $^3P_0 \rightarrow {}^3H_4$ emission, while in $CaTiO_3$ shows a single red $^1D_2 \rightarrow {}^3H_4$ luminescence [6]. Due to these tunable emission properties, previous works have suggested the use of some Pr^{3+}-doped oxides in solid-state lighting, sensor, and optical-electro integration [7,8].

On the other hand, in order to explain the mechanism of the de-excitation pathways that contribute to partial or total quenching of $^3P_0$ luminescence in oxide-based lattices, some models have been proposed [9,10]. In these models, it is explained that at least, the rate of $^3P_0 \rightarrow {}^1D_2$ radiationless relaxation is induced by multiphonon process and depends on the phonon energy of the host lattice, and in the case of Pr^{3+} is known to be rather high compared to most of the other rare earth ions [11]. This rate is also greatly affected by the Pr^{3+} amount and by the uniform distribution of the ions in the host lattice. Additionally, in the case of Pr^{3+}-doped titanates, it is possible to expect a charge transfer state Pr^{4+}-O^{2-}-Ti^{3+} close to excited states of Pr^{3+}-O^{2-}-Ti^{4+} configuration, called the intervalence charge transfer band (IVCT). So, that relaxation occurs in this intermediate state and then the electron returns to the Pr^{3+} ion in the excited $^1D_2$ state [12]. Also, in some reports the PL intensity and performance or afterglow were studied, and it is stated that they are dependent on the Pr^{3+} concentration. In this case the optimal concentration of Pr^{3+} ions for the brightest PL emission and the best afterglow characteristic were experimentally found to be 0.5 mol% and 0.4 mol% in $SrZrO_3$:Pr^{3+} [13].

* Corresponding author.
E-mail address: fgg@xanum.uam.mx (F. González).

http://dx.doi.org/10.1016/j.jlumin.2017.07.048
Received 7 May 2017; Received in revised form 25 July 2017; Accepted 26 July 2017
Available online 27 July 2017

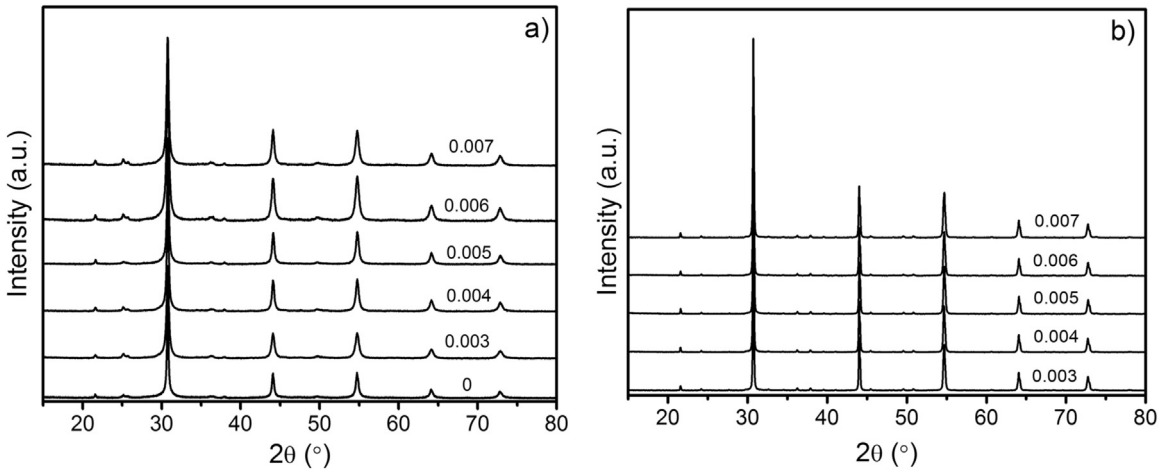

Fig. 1. XRD of $Sr_{1-1.5x}Pr_xZrO_3$ powders synthesized by Pechini method and calcined at: (a) 800 °C for 1 h and (b) 1400 °C for 2.

In this work, the relationship between crystalline structure, microstructure and luminescent properties of Pr^{3+} doped $SrZrO_3$ prepared by two different methods, were studied.

2. Experimental

2.1. Synthesis of ceramic powders

For the preparation of zirconate powders the Pechini and solid-state methods were used. The Pechini method involves the preparation of a polymeric resin from organic acids, alcohols and the ions required for the desired material. Both, the acid and alcohol must be poly-functional compounds for preparing a desirable three-dimensional polymeric network [14–16]. For the Pechini method the raw materials used were high purity reagent of $Sr(NO_3)_2$ (99.0%, Sigma-Aldrich), $ZrO(NO_3)_2{\cdot}6H_2O$ (99.0%, Sigma-Aldrich), $Pr(NO_3){\cdot}6H_2O$ (99%, Sigma-Aldrich), citric acid monohydrate (99%, JT Baker) and ethylene glycol (99%, Sigma-Aldrich). The nitrates were dissolved into deionized water, then citric acid and ethylene glycol were added. The nominal molar ratio of the mixed solutions were 1:5 of [total amount of metals ions]: [citric acid]. This solution was heated at 70 °C for dehydration and at 100 °C for polymerization. Thermal pyrolysis was carried out by heating the polymerized resin at temperatures between 700 °C and 1400 °C for 1–2 h in air. For the synthesis of the sample containing 1 mol% of Ti^{4+} $C_{12}H_{28}O_4Ti$ was used (Sigma-Aldrich 97%), and almost the same procedure as described above, but deionized water was replaced by absolute ethanol as the solvent.

For the traditional high temperature, solid-state reaction, the starting materials were $SrCO_3$ (99.99%, Sigma-Aldrich), ZrO_2 (99.0%, Sigma-Aldrich), and Pr_6O_{11} (99.99%, Sigma-Aldrich) [17]. The raw materials were weighed in the stoichiometric proportion according to the nominal compositions of $Sr_{1-1.5x}Pr_xZrO_3$ (x = 0.003, 0.004, 0.005). Then, the powders were mixed and milled thoroughly for 30 min in agate mortar and calcined at 750 °C for 1 h, then further at 1200 °C and 1400 °C for 2 h in air, respectively.

2.2. Structural and microstructural characterization

Crystal structure identification of $Sr_{1-1.5x}Pr_xZrO_3$ powders were carried out by X-ray diffraction (Bruker D8 Advance with Cu Kα). Patterns were recorded in 2θ range of 20–80°. Rietveld refinement was performed with the Maud software, using crystallographic data reported [18,19]. The microstructure of the samples and the EDS spectrum were performed using a Scanning Electron Microscope (JEOL JSM IT300).

2.3. Luminescent properties

The optical characterization of crystalline powders was performed acquiring the emission and excitation spectra, which were recorded with an Edinburg Instruments FSP920 spectrofluorometer based on the method of single photon counting which combines steady state and phosphorescence lifetime measurements. The spectrofluorometer is equipped with a 450 W xenon lamp as a CW light source and R928P PMT as a detector. In order to avoid the light dispersion, a double monochromator (two coupled 0.3 m) was employed to excite the samples. All the excitation and emission spectra were corrected for the wavelength dependent responses of the Xe-lamp and the detector, respectively. The spectra were recorded in the wavelength range between 250 nm and 775 nm. For the measurements of luminescence decay, the excitation photons were provided by a 60 W μF920H pulsed Xe flash-lamp with a pulse width of ~ 1.5 μs and a repetition rate of 100 Hz. All measurements were carried out at room temperature. The absorption spectra were obtained by using the diffuse reflectance technique. The measurements were performed in a Cary 5 spectrophotometer equipped with a Praying Mantis (Harrick Scientific Products, Inc.) accessory for diffuse reflection spectroscopy. The spectra were recorded in the wavelength range between 200 nm and 650 nm.

3. Results and discussion

The XRD results for samples prepared by Pechini method calcined at 800 °C and 1400 °C are shown in Fig. 1(a) and (b), respectively. Pure perovskite phase was obtained in all the compositions and calcined temperatures; this is possible due to the mixing of the reagents at atomic level achieved by Pechini method. It is well-known that the polymerization aids the homogeneous distribution of cations, lowering the required energy for the crystallization. Furthermore, the low temperature crystallization allows the preparation of nanocrystalline powders. In general, the intensities of XRD peaks increase with higher calcination temperature, which indicates an increase in the crystallite size. The effect of Pr^{3+} ions (at the studied concentrations, which are very low) on $SrZrO_3$ lattice seems to be negligible as XRD patterns remain the same at different doping concentrations for each temperature. In order to analyze the effects of the temperature and the Pr^{3+} doping concentration on the crystal structure and the average crystallite size, we performed Rietveld refinements. The unit cell of the $SrZrO_3$ was modelled with orthorhombic symmetry described by the space group *Pnma* (62), and a basis containing one Zr^{4+}, one Sr^{2+} and two O^{2-} at the relative coordinates (0, 0, 0), (x, y, ¼), (x_{O1}, y_{O1}, ¼) and (x_{O2}, y_{O2}, z_{O2}), respectively. The initial values for cell parameters and atomic coordinates were set according to Kennedy et al. [20].

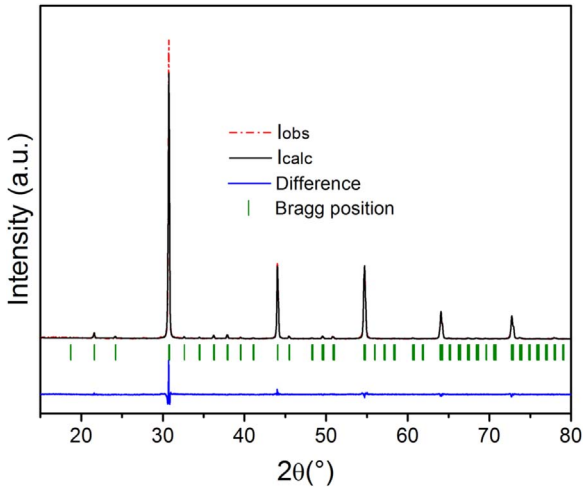

Fig. 2. Rietveld refinement plot of $Sr_{0.991}Pr_{0.006}ZrO_3$ powders synthesized by Pechini method and calcined at 1400 °C for 2 h.

Table 1
Rietveld refinement results for samples synthesized by Pechini method and calcined at 800 °C, 1200 °C and 1400 °C.

Samples calcined at 800 °C	Lattice parameters			Crystallite Size	R_{wp}
	a (Å)	b (Å)	c (Å)	(nm)	
$Sr_{0.9955}Pr_{0.003}ZrO_3$	5.822(1)	5.800(1)	8.192(1)	31.2(3)	12.00
$Sr_{0.994}Pr_{0.004}ZrO_3$	5.803(1)	5.816(1)	8.201(1)	43.2(5)	12.54
$Sr_{0.9925}Pr_{0.005}ZO_3$	5.808(4)	5.809(4)	8.201(1)	44.2(2)	12.07
$Sr_{0.991}Pr_{0.006}ZrO_3$	5.820(1)	5.800(1)	8.194(1)	33.2(3)	11.34
1200 °C					
$Sr_{0.9955}Pr_{0.003}$ ZrO_3	5.808(4)	5.821(4)	8.214(6)	166(2)	10.54
$Sr_{0.994}Pr_{0.004}ZrO_3$	5.806(3)	5.821(3)	8.208(4)	157(1)	9.75
$Sr_{0.9925}Pr_{0.005}ZrO_3$	5.807(3)	5.821(3)	8.210(5)	157(2)	9.80
$Sr_{0.9895}Pr_{0.007}ZrO_3$	5.791(5)	5.815(2)	8.226(3)	151(2)	9.39
1400 °C					
$Sr_{0.9955}Pr_{0.003}$ ZrO_3	5.802(2)	5.818(2)	8.214(4)	514(12)	11.54
$Sr_{0.994}Pr_{0.004}ZrO_3$	5.805(2)	5.819(2)	8.213(4)	588(27)	11.95
$Sr_{0.9925}Pr_{0.005}$ ZrO_3	5.803(2)	5.818(2)	8.211(3)	514(22)	11.00
$Sr_{0.991}Pr_{0.006}ZrO_3$	5.803(2)	5.819(2)	8.211(3)	514(16)	10.46
$Sr_{0.9895}Pr_{0.007}$ ZrO_3	5.799(5)	5.818(2)	8.219(3)	570(2)	11.19

In Fig. 2, a typical Rietveld refinement plot is shown. It corresponds to sample $Sr_{0.991}Pr_{0.006}ZrO_3$ calcined at 1400 °C for 2 h. It can be seen a good matching between the experimental data and the proposed model. The results of the Rietveld analysis for the structural parameters ***a***, ***b*** and ***c***, and the average crystallite size as a function of Pr^{3+} content are displayed in Table 1.

A shallow dependence with x is manifested, which suggests the incorporation of Pr^{3+} into the $SrZrO_3$ crystal structure. These results agree with those reported in the literature [19,20].

To compare the results obtained by Pechini method with those obtained by solid state method, the following compositions were prepared: $x = 0.003$, 0.004 and 0.005.

The XRD results for these samples calcined at 1400 °C are shown in Fig. 3. The results of Rietveld refinement analysis are shown in Table 2. It is observed that the cell parameters are like those obtained by Pechini method, but there is a notable increment in the crystallite size (from 0.588 ± 0.027 μm to 1.556 ± 0.170 μm) which is evidenced by the increment in the XRD relative intensity. The samples calcined at 1200 °C are not completely pure (they have ZrO_2 secondary phase, JCPDS No. 49-1746) but it apparently reacts at all when the powders were further calcined at 1400 °C for 2 h, since it is not detected in the X-ray patterns.

The particle size, morphology, composition and stoichiometry together play an important role in the performance of phosphor materials

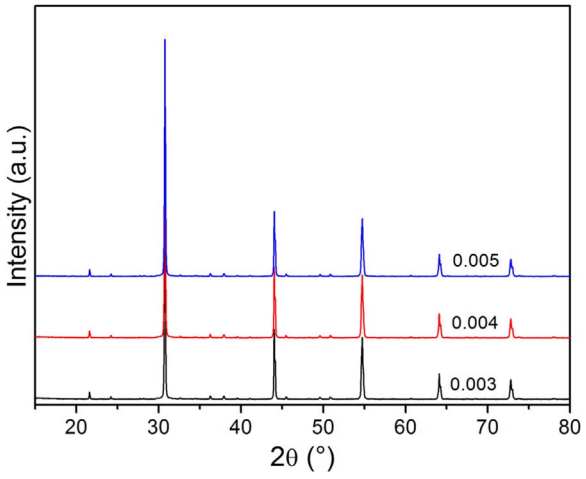

Fig. 3. XRD of $Sr_{1-1.5x}Pr_xZrO_3$ powders prepared by solid state method and calcined at 1400 °C for 2 h.

Table 2
Rietveld refinement results for samples synthesized by solid state method and calcined at 1400 °C for 2 h.

Sample	Cell parameters			Crystallite Size (nm)	R_{WP}
	a (Å)	b (Å)	c (Å)		
$Sr_{0.9955}Pr_{0.003}ZrO_3$	5.799(1)	5.814(1)	8.209(2)	1420(142)	13.63
$Sr_{0.994}Pr_{0.004}ZrO_3$	5.799(1)	5.814(1)	8.208(2)	1556(169)	13.50
$Sr_{0.9925}Pr_{0.005}ZrO_3$	5.799(1)	5.814(1)	8.208(3)	1423(149)	12.57

as those reported here, SEM studies were carried out to investigate the surface morphology of the Pr^{3+}-doped $SrZrO_3$ phosphors. Fig. 4(a), (b) and (c), present images of the samples synthesized by Pechini method calcined at 700 °C, 800 °C and 1400 °C, respectively. In this case particle size increased while agglomeration decreased with increasing synthesis temperature. At 1400 °C it can be seen particles uniformly distributed and the crystallites have uniform shapes and sizes. The particle size cannot be measured exactly from the SEM image; however, it is evident that the average particle sizes for all the samples are less than 0.2 μm which is comparable with the results of Rietveld refinement (~ 0.5 μm average crystal size).

Fig. 4(d) and (e) show the SEM images of the samples synthesized by solid-state method. It is observed that the as-prepared powders exhibit small particles forming spherical agglomerates. The sizes of particles are less than 2.5 μm. Clearly, the particle sizes do not show an evident increase with the increasing in the annealing temperature from 1200 °C to 1400 °C. In the design of powder phosphors, the ideal morphology is that of a perfect sphere [3], the need for spherical particles has already been recognized for some time, and modified round-particles have been used in high voltage CRT applications [4,5]. The luminescence properties of phosphor particles depend on the characteristics of the particles such as size, shape, crystallinity, defects and so on.

The excitation spectra of samples prepared by Pechini method when monitoring the 489 nm ($^3P_0 \rightarrow {}^3H_4$) emission of Pr^{3+} in $SrZrO_3$ are presented in Fig. 5. The curves shape is similar for all samples, but the relative intensities increase monotonously with a maximum at $x = 0.006$ and then decreases for $x = 0.007$. Several excitation peaks in the range 430 nm − 480 nm due to *f-f* transition of Pr^{3+} are observed. There are two main peaks around 451 nm and 469 nm which can be assigned to the transitions from $^3H_4$ energy level to $^3P_2$ and ($^3P_1$, $^1I_6$) levels, respectively [2,13]. In addition, the weak broad band between 250 nm and 275 nm is also observed. This band can be ascribed to the absorption of $SrZrO_3$ host [13].

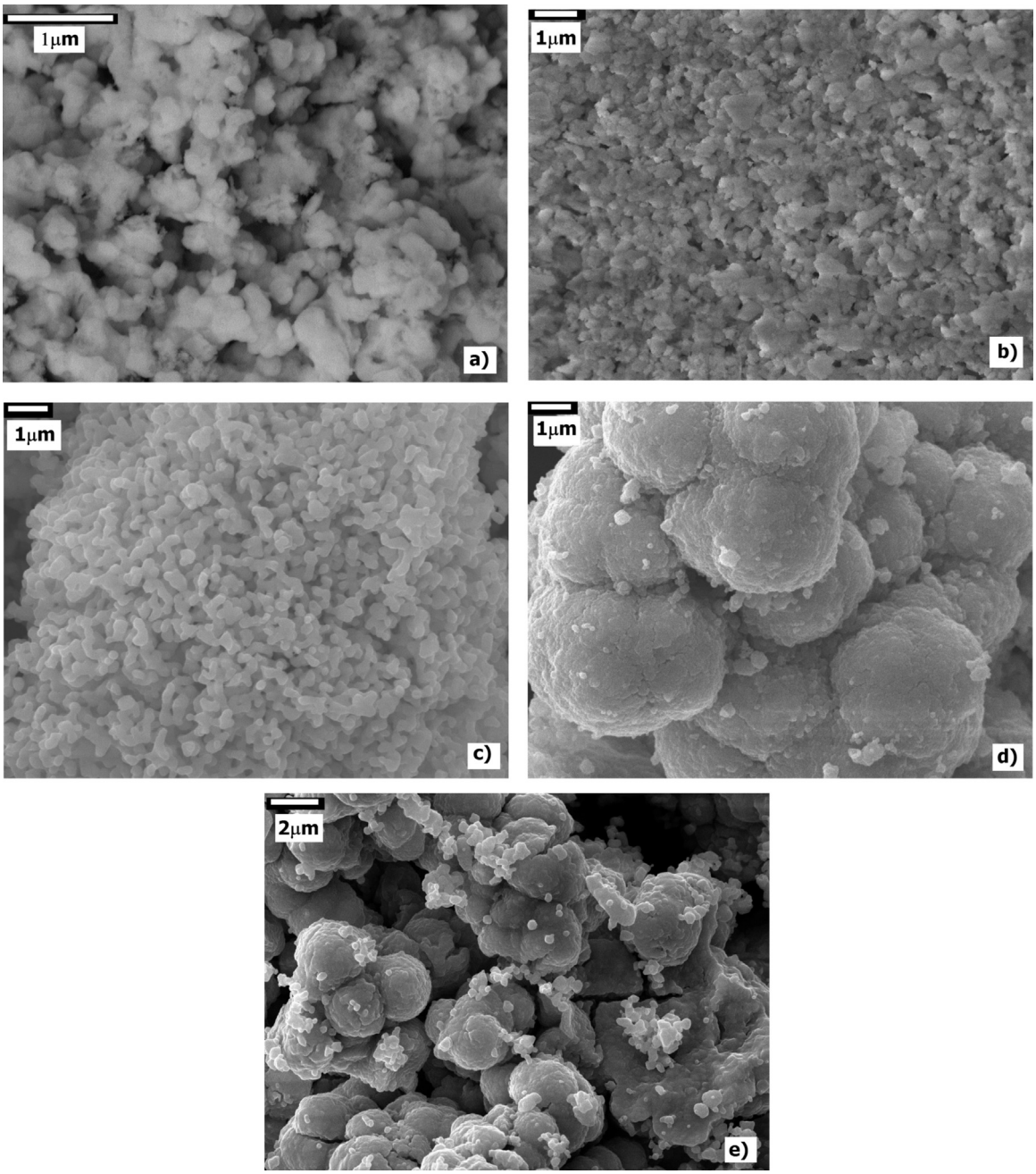

Fig. 4. SEM images of $Sr_{0.991}Pr_{0.006}ZrO_3$ prepared by Pechini method calcined at (a) 700 °C, (b) 800 °C (c) 1400 °C and $Sr_{0.994}Pr_{0.004}ZrO_3$ prepared by ceramic method calcined at (d) 1200 °C 2 h, (e) 750 °C 1 h + 1200 °C 2 h + 1400 °C 2 h.

Fig. 6(a) shows the emission spectra (λ_{ex} = 446 nm, $^3H_4 \rightarrow {}^3P_2$) of all $SrZrO_3$:Pr^{3+} samples prepared by Pechini method. The spectra consist of sharp lines in the region (400 nm–775 nm). There are several emission peaks, localized at (around) 489, 532, 546, 607, 619, 631, 652, 689, 713 and 738 nm that correspond to the $^3P_0 \rightarrow {}^3H_4$, $^3P_1 \rightarrow {}^3H_5$, $^3P_0 \rightarrow {}^3H_5$, $^1D_2 \rightarrow {}^3H_4$, $^3P_0 \rightarrow {}^3H_6$, $^3P_1 \rightarrow {}^3F_2$, $^3P_0 \rightarrow {}^3F_2$, $^3P_1 \rightarrow {}^3F_3$, $^3P_0 \rightarrow {}^3F_3$ and $^3P_0 \rightarrow {}^3F_4$ transitions.

These results agree with previous reports [20,21]. The increasing in relative intensity observed in Fig. 6(a), corroborates that increasing calcination temperature, enhances the luminescence response.

The effect of Pr^{3+} content on the luminescence intensity of $Sr_{1-1.5x}Pr_xZrO_3$ phosphors synthesized by Pechini method when excited at λ_{ex} = 446 nm, could be better appreciated in Fig. 6(b). In general, it is observed that the emission intensity increases with higher calcination temperature and Pr^{3+} content and reaches a maximum value for x = 0.006. Higher doping concentrations, result in the enhancement of non-radiative relaxation between the neighboring Pr^{3+} ions, which produces concentration quenching [13].

The excitation spectra of samples prepared by solid state method when monitoring the emission of the $^3P_0 \rightarrow {}^3H_4$ transition at 489 nm of Pr^{3+} in $SrZrO_3$ are presented in Fig. 7. As it is shown, the peaks ascribed to *f-f* transitions are similar to the excitation spectra of samples prepared by Pechini method, however, now, it is observed a noticeable strong and broad band between 250 nm and 300 nm with a maximum at ~260 nm.

Trying to elucidate its origin, different possibilities such as the presence of a small amount of ZrO_2 not revealed in X-ray patterns, and the presence of other impurities were considered. According to the EDS spectrum showed as an inset in Fig. 7, we conclude that the presence of a very small amount of Ti^{4+} in the zirconium oxide used as precursor is

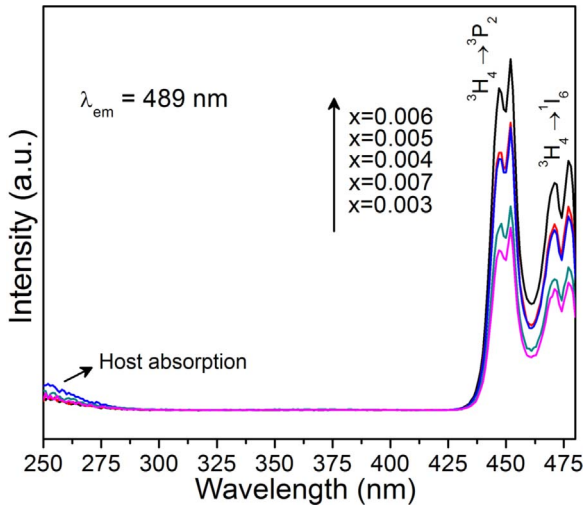

Fig. 5. Excitation spectra (λ_{em} = 489 nm) of $Sr_{1-1.5x}Pr_xZrO_3$ samples synthesized by Pechini method and calcined at 1400 °C.

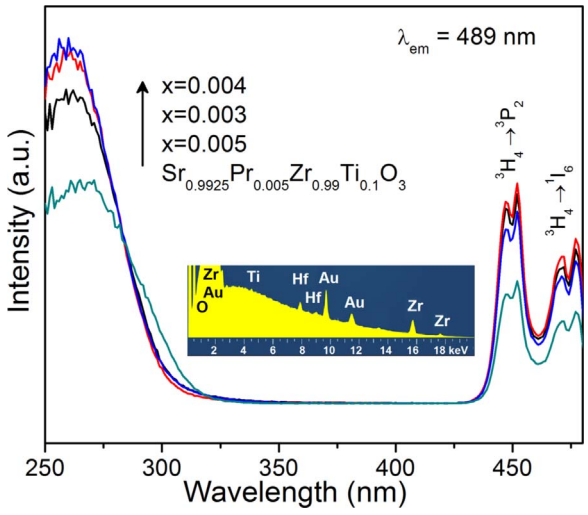

Fig. 7. Excitation spectra (λ_{em} = 489 nm) of the samples synthesized by solid-state method and the sample synthesized by Pechini method containing 1 mol% of Ti^{4+}. Inset shows the EDS spectrum of the ZrO_2 (coated with gold) used as precursor in the solid-state method.

the cause of this band. To support this finding, we synthesized a sample containing 1 mol% of Ti^{4+} by the Pechini method. The excitation spectrum of this sample is also showed in Fig. 7. The appearance of the band when Ti^{4+} is present is due to a charge transfer band (CTB), originated from the transfer of an electron of the valence band to Ti^{4+}, which have been reported in oxides containing Ti^{4+} [22–24].

According to the chemical shift model (CSM) formulated by Dorenbos [25,26], it is possible to assess the location of the top and bottom of the valence and conduction bands, respectively, as well as the location of the 4f-energy-levels of divalent and trivalent lanthanides, all they referred to a unique energy reference: the vacuum binding energy (VBE). More recently it has also been shown that it is possible to include in this scheme the energy $Ti^{3+/4+}$ donor-acceptor states [27], which is useful to locate the $O^{2-} \rightarrow Ti^{4+}$ CT transition, referred to the VBE.

Thus, using this approach, we can explain our results of luminescent spectroscopy, in good agreement with the CSM. From the data reported in ref [28] we have constructed the vacuum referred binding energy (VRBE) scheme (and consequently the host referred binding energy (HRBE)) of Pr^{3+} incorporated into $SrZrO_3$ which is presented in Fig. 8(a). Since the energy associated with the $O^{2-} \rightarrow Ti^{4+}$ CTB provides the location of the Ti^{3+} $3d_1$ ground state above the valence band energy E_v [27], we have measured diffuse reflectance spectra (shown in Fig. 8(b)) of some representative samples to place Ti^{3+} $3d_1$ state in Fig. 8(a). In the absence of Ti^{4+} impurities, i.e., when Pechini method is used, the only expected transitions correspond on the one hand to that of the host, and on the other to those of Pr^{3+}. Excitation spectra depicted in Fig. 5 are in accordance with this result. In Fig. 8(a), arrow 1 represents the transition from an electron in the top of the valence band to the energy level of the host exciton, the value of 5.8 eV agrees well with the small band at the edge of short wavelengths in Fig. 5 and with the sharp well-defined bands of diffuse reflectance spectra of Fig. 8(b) having maxima at 219 nm (~ 5.66 eV), especially if the values of the VRBE are considered to have typical errors of around 0.1 eV and, additionally, that the value of the excitation energy is measured or estimated considering a temperature of 10 K [28]. Arrows 2 correspond to *f-f* transitions of Pr^{3+} which are also observed in Fig. 5. Arrow 3, represents the CT transition between O^{2-} and Ti^{4+} and its value of 4.75 eV and 4.90 eV, obtained from the maxima at ~ 260 nm and ~ 250 nm of excitation spectra (Fig. 7) and diffuse reflectance spectra (samples $Sr_{0.9925}Pr_{0.005}Zr_{0.99}Ti_{0.01}O_3$ synthesized by Pechini method and $Sr_{0.9925}Pr_{0.005}ZrO_3$ synthesized by solid state reaction in Fig. 8(b)), respectively: This value agrees well with those ones found in oxide compounds possessing isolated titanate groups [23–25,27]. In Fig. 7, are also observed the *f-f* transitions of the Pr^{3+} corresponding to arrows 2 in Fig. 8(a).

In Fig. 9(a) the emission spectra for all samples synthesized by the

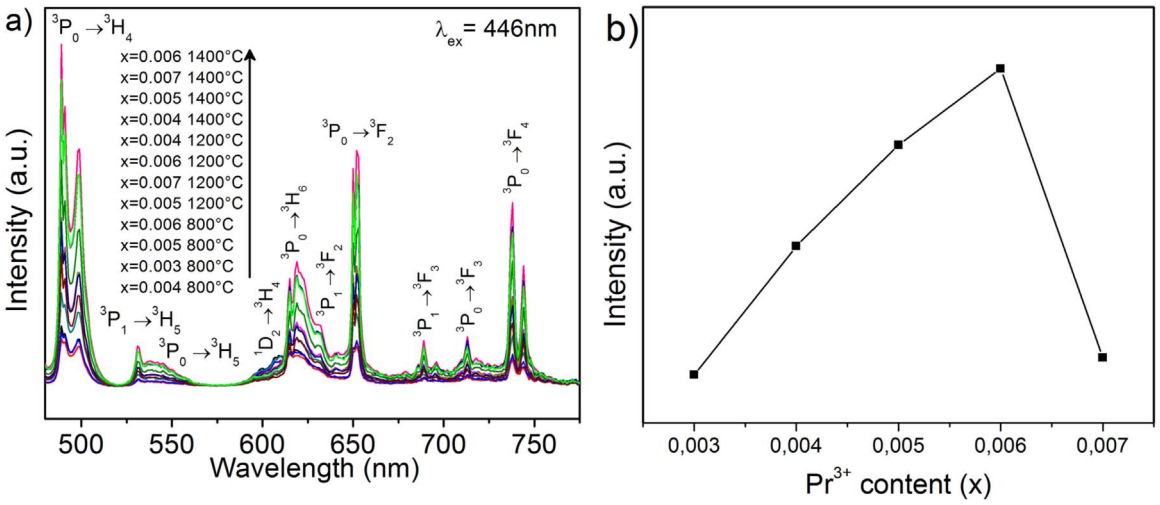

Fig. 6. Emission spectra (λ_{ex} = 446 nm) a), and emission intensity at the maxima as a function of the Pr^{3+} content for samples synthesized by Pechini method calcined at 1400 °C.

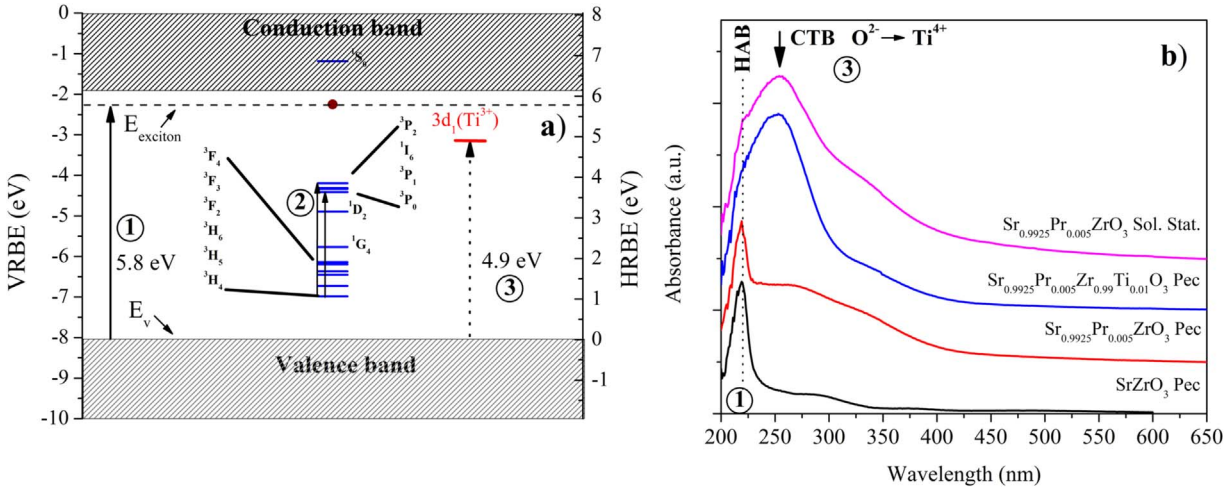

Fig. 8. Host referred (right-hand energy scale) and vacuum referred (left-hand energy scale) binding energy schemes for Pr^{3+} in $SrZrO_3$ (a). Diffuse reflectance spectra of some representative samples (b). At low wavelength values appears the host absorption band (HAB). CTB from the valence band to $3d_1$ of Ti^{3+} is observed around 250 nm.

solid-state method are depicted. A similar behavior as that exhibited in samples synthesized by Pechini method is observed; thus, when samples were excited through $^3H_4 \rightarrow {}^3P_2$ (λ_{ex} = 446 nm) the greenish blue transition dominates the emission response, and many other emission peaks ascribed to $^3P_{1,0} \rightarrow {}^{2S+1}L_J$ transitions, are also observed. Moreover, in a more remarkable way than in the case of the samples synthesized by Pechini method (Fig. 9(b)), the emission rises when calcination temperature increases, and again an optimum is reached for a given composition (x = 0.004). However, when these samples and that one synthesized by Pechini method containing Ti^{4+} at 1 mol% were excited through the $O^{2-} \rightarrow Ti^{4+}$ CTB (λ_{ex} = 250–300 nm), noticeably emission associated with the $^1D_2 \rightarrow {}^3H_4$ transition gains intensity. To illustrate this fact, in Fig. 10 are shown emission spectra of samples $Sr_{0.9925}Pr_{0.005}ZrO_3$ prepared by solid state reactions (Fig. 10(a)) and $Sr_{0.9925}Pr_{0.005}Zr_{0.99}Ti_{0.01}O_3$ prepared by Pechini method (Fig. 10(c)) when excited at different wavelengths of the CTB. Comparison of normalized emission spectra when each of these samples is excited at 446 nm and at 260 nm are shown in Fig. 10(b) and (d). The gain in the intensity of emission ascribed to the $^1D_2 \rightarrow {}^3H_4$ transition would appear to be analogous to the case of titanates doped with Pr^{3+}, in which this transition dominates the emission of Pr^{3+} due to the presence of an IVCT. However, no evidence in the excitation spectra (Fig. 7) of the $Pr^{3+} \rightarrow 3d_1(Ti^{4+})$ transition, which would be expected as a peak at ~ 325 nm (see Fig. 8(a)) and being the analogue to the Pr^{3+}-IVCT process in titanates, is observed. Certainly, this process must be negligible because of the low contents of Pr^{3+} and Ti^{4+}. Thus, we think other energy-transfer mechanism involving $Ti^{4+} \rightarrow O^{2-}$ CT transition is responsible for the relative increase of the emission associated with the $^1D_2 \rightarrow {}^3H_4$ transition. Perhaps this energy transfer is mediated by defects whose presence is discussed below.

Interesting to notice is the wide emission band between 350 nm and 475 nm. It position resembles those ones reported in similar compounds for a reverse $Ti^{4+} \rightarrow O^{2-}$ CT transition [29,30]; however, since it quenches at low temperature, we are inclined to think that another mechanism involving defects is responsible for this broad band emission. In our opinion this possibility is supported by the tails in diffuse reflectance spectra of Fig. 8(b). This absorption on the long-wavelength side of the absorption edge, even in the pure sample, and because of its remarkable increase by the addition of Pr^{3+} and its relative intensity depending on the synthesis method (Fig. 10(b) and (d)), it seems to be related to oxygen vacancies [31]. The change in the shape of the wide emission band going in excitation wavelengths from 250 nm to 300 nm is attributed to the presence of an amount of unreacted ZrO_2 (imperceptible through XRD). The emission spectrum of ZrO_2 used in the synthesis of samples by the solid-state method is shown at the top of the Fig. 10(a). It is possible to realize that its contribution is present in the

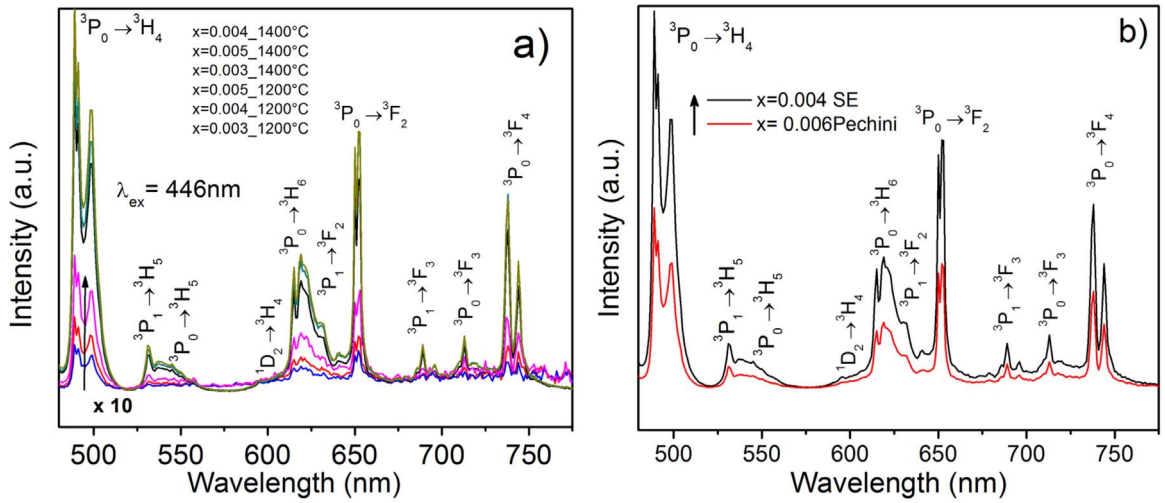

Fig. 9. Emission spectra (λ_{ex} = 446 nm) of samples synthesized by solid state method calcined at 1200 °C and 1400 °C (a). Comparison of the emission spectra (λ_{ex} = 446 nm) of samples calcined at and 1400 °C with the best luminescent performance depending on the synthesis method (x = 0.004 for solid state, and x = 0.006 for Pechini route) (b).

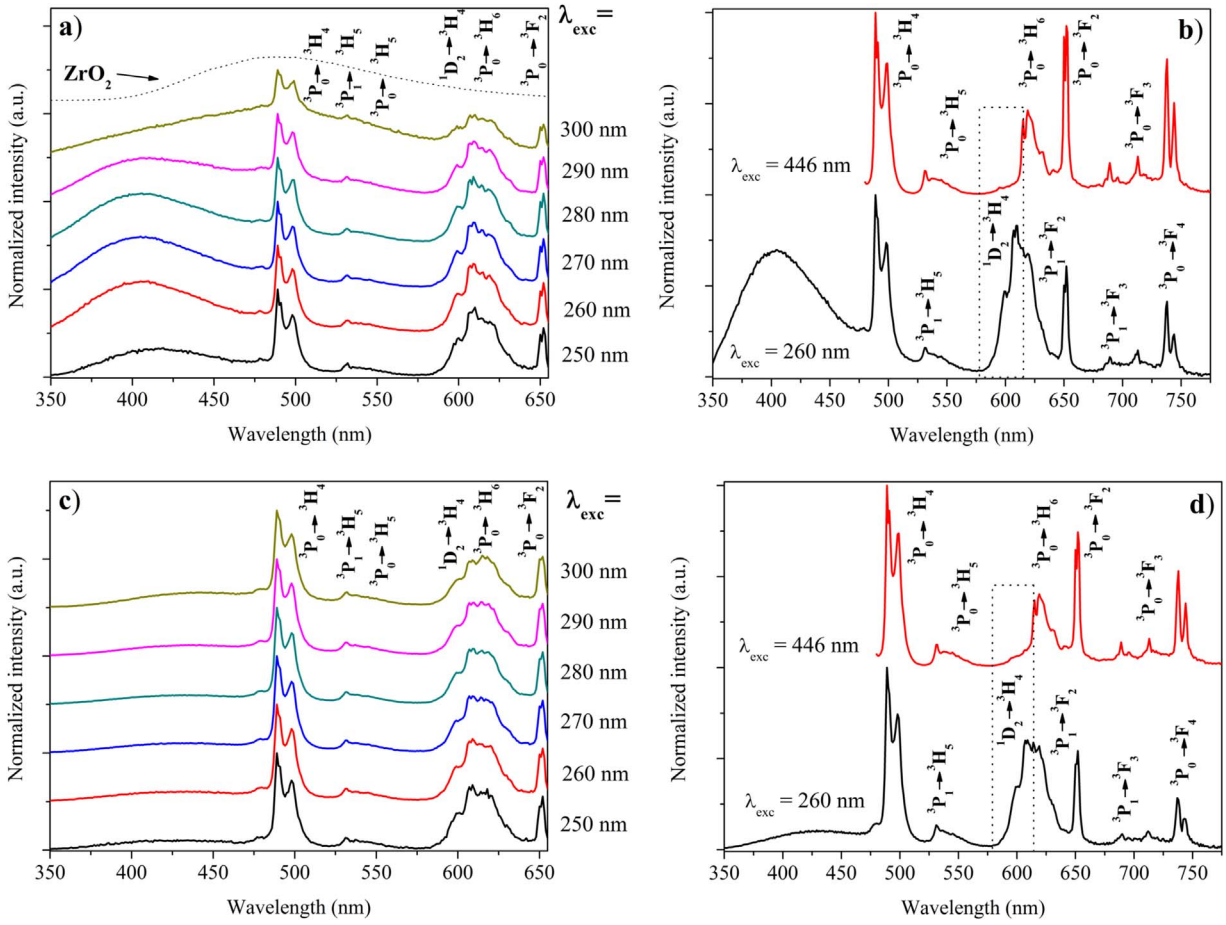

Fig. 10. Emission spectra of samples $Sr_{0.9925}Pr_{0.005}ZrO_3$ prepared by solid state reactions (a) and (b), and $Sr_{0.9925}Pr_{0.005}Zr_{0.99}Ti_{0.01}O_3$ prepared by Pechini method ((c) and (d). In (a) and (c) exciting at different wavelengths of the CTB. In (b) and (d) comparison of the relative intensity of emission assigned to the $^1D_2 \rightarrow {}^3H_4$ transition when exciting at 260 nm and at 446 nm; also, the relative intensity of the broad emission band depending on the synthesis method is observed. ZrO_2 in (a) corresponds to the emission spectrum (λ_{exc} = 300 nm) of monoclinic ZrO_2 used as precursor in solid state synthesis.

emission spectra when sample $Sr_{0.9925}Pr_{0.005}ZrO_3$ is excited at 290 nm and so evident when exciting at 300 nm.

The improvement in luminescence of samples prepared for both synthesis methods can be explained as due to the growth of crystallite size when increasing temperature, resulting in the reduction of (micro) structural defects which can act as annihilation sites for luminescence; and also, that reduction promotes the decrease of light scattering from the surfaces and interfaces [32].

To support these affirmations, we performed measurements of luminescence decay curves in samples with different composition prepared for both methods, and calcined at different temperatures.

Luminescence decay curves of samples calcined at 1400 °C are also useful to explain the concentration quenching effect on the luminescent response. All measurements were done using the optimum excitation and emission wavelengths for each sample.

In Fig. 11 are plotted the luminescence decay curves for different samples synthesized by the Pechini (Fig. 11(a)) and solid state (Fig. 11(b)) methods. All plots, with the only exception of the sample synthesized by Pechini method and calcined at 800 °C, show an exponential decay profile. We attribute the non-exponential decay behavior of sample calcined at 800 °C to a larger contribution of non-radiative processes, originated in a more distorted environment, since this sample has the smallest crystallites (see Table 1) and thus, in principle, more microstructural defects are present.

In the case of the samples synthesized by the Pechini method, it is observed, even though the Pr^{3+} content is the same, that if calcination temperature increases, then according to equation

$$\tau_{meas} = \frac{1}{A_R + A_{NR}}$$

where τ_{meas}, A_R and A_{NR}, are the measured lifetime, the radiative and the non-radiative decay rates, respectively, and assuming that A_R is constant for all samples, that the non-radiative mechanism should be inhibited, and therefore the measured lifetimes must increase. In Table 3, are shown the values of τ_{meas}, for each decay curve plotted in Fig. 11.

Regarding significant discrepancies between red spectral region of emission spectra obtained previously and those ones obtained in the present work, in Fig. 12 are shown the corrected and uncorrected emission spectra of the $Sr_{0.994}Pr_{0.004}ZrO_3$ sample synthesized by Pechini method.

As it is observed, correcting emission spectra for the wavelength dependent response of the detector has the main impact on the red spectral region. Thus, we conjecture this may be the origin of the differences. When talking about phosphors, this is not a minor issue since these types of spectra are often used for the assignment of CIE color coordinates, and inappropriate measurement of relative emission intensities may lead to incorrect results.

4. Conclusions

It was found that the Pechini method reduces the synthesis temperature and time for preparing Pr^{3+} doped $SrZrO_3$ powders. This preparation method allows us to obtain a pure perovskite phase. On the other hand, powders prepared by the solid-state method showed better

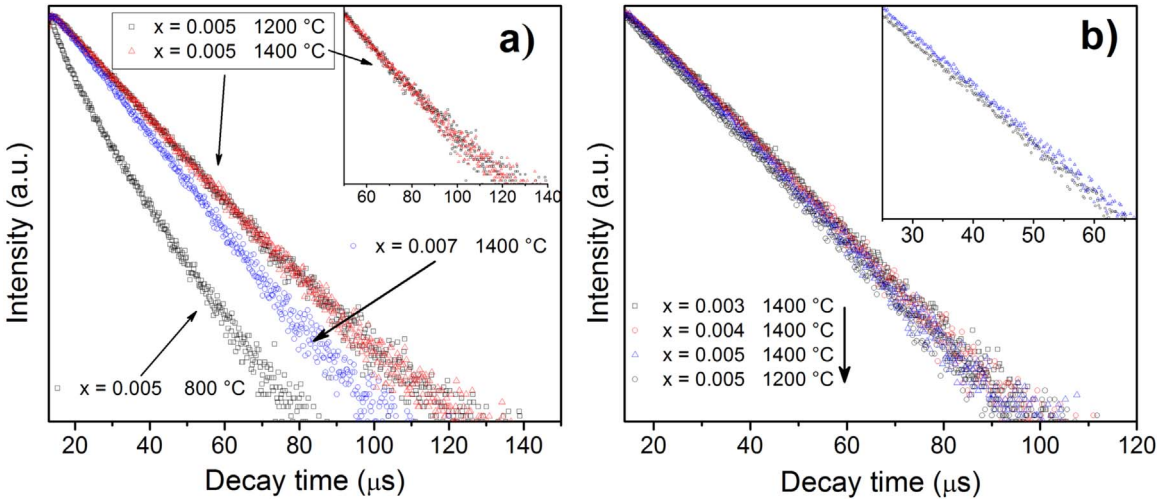

Fig. 11. Luminescence decay curves for samples synthesized by Pechini (a) and solid-state (b) methods.

Table 3
Decay data for some studied compositions.

Synthesis method	x (mol)	Sintering temperature (T /°C)	τ_{meas} (μs)
Pechini	0.005	800	3.99(14)
			11.87(8)[a]
		1200	16.80(3)
		1400	16.83(3)
	0.007	1400	14.25(2)
Solid state	0.003	1400	13.61(2)
	0.004	1400	13.36(2)
	0.005	1200	12.94(2)
		1400	13.02(2)

[a] There are two values for lifetime because due to the non-exponential luminescence decay of this sample we fitted its curve using the equation $I(t) = A_1 e^{-\left(\frac{t}{\tau_1}\right)} + A_2 e^{-\left(\frac{t}{\tau_2}\right)}$. In the other samples we used a single exponential decay for fitting curves.

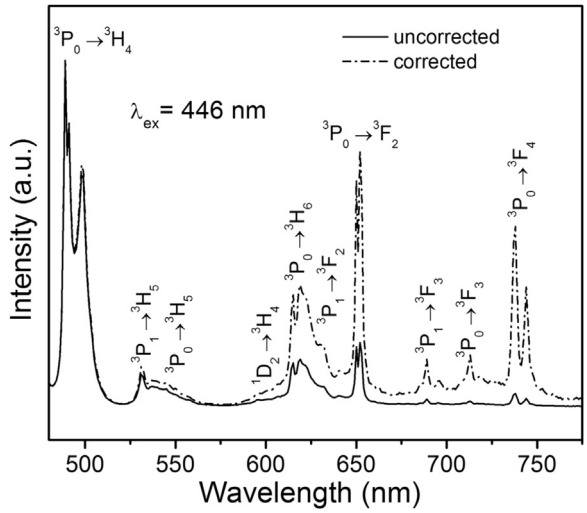

Fig. 12. Comparison in the emission spectra of the $Sr_{0.994}Pr_{0.004}$ ZrO_3 sample with and without correction.

luminescent response; furthermore, the luminescence ascribed to the $^1D_2 \rightarrow {}^3H_4$ transition of Pr^{3+} is significantly increased in these samples when excited through the $O^{2-} \rightarrow Ti^{4+}$ CTB, by the presence of Ti^{4+} as impurity. This result was corroborated in a sample synthesized by Pechini method and deliberately doped with Ti^{4+} at 1 mol%. No evidence about the increase of the $^1D_2 \rightarrow {}^3H_4$ transition through the state $Pr^{3+}/Ti^{4+} \rightarrow Pr^{4+}/Ti^{3+}$ ($^3H_4(Pr^{3+}) \rightarrow 3d_1(Ti^{3+})$) was found. Additionally, in samples prepared by the solid-state method, even though the XRD analysis show no secondary phases, the existence of unreacted ZrO_2 was confirmed by the luminescence results. From luminescence decay curves, the enhancement of Pr^{3+}-luminescence due to the increase in the calcination temperature of all samples is explained because the reduction of non-radiative processes associated with the improvement in crystal size and the diminishment of defects, which may act as quenching centers. Important to emphasize is the need of correcting luminescence spectra for comparison purpose and potential applications. In summary, the original contributions of the present work are the low temperature synthesis of compounds, and the understanding of some interesting luminescent properties of the Pr^{3+}-doped $SrZrO_3$ system; namely, the CTB due to the presence of Ti^{4+}, the incomplete inhibition of the red emission band, an the fact that exciting through CTB actives significantly the emission associated with the $^1D_2 \rightarrow {}^3H_4$ transition.

Acknowledgments

T. J. Pérez-Juache is grateful to CONACYT for the postdoctoral scholarship granted. The authors thank LDRX (T 128) UAM-I for XRD measurements; Orlando Hernández Cristobal and Neftalí Razo-Pérez for EDS analysis and SEM images, and technical assistance, respectively.

References

[1] N.S. Lewis, D.G. Nocera, Powering the planet: chemical challenges in solar energy utilization, Proc. Natl. Acad. Sci. USA 103 (2006) 15729–15735.
[2] G.H. Dieke, Spectra and Energy Levels of Rare Earth Ions in Crystals, Wiley, New York, 1968.
[3] P. Boutinaud, L. Sarakha, E. Cavalli, M. Bettinelli, P. Dorenbos, R. Mahiou, About red afterglow in Pr^{3+} doped titanate perovskites, J. Phys. D: Appl. Phys. 42 (2009) 45106 (7 pp).
[4] B. Lei, B. Li, H. Zhang, L. Zhang, Y. Cong, W. Li, Synthesis and luminescence properties of cube-structured $CaSnO_3$ / RE^{3+} (RE = Pr, Tb) long-lasting phosphors, J. Electrochem. Soc. 154 (2007) H623–H630.
[5] Z. Liu, Y. Liu, J. Zhang, J. Rong, L. Huang, D. Yuan, Long afterglow in Pr^{3+} and Li^+ co-doped $CaZrO_3$, Opt. Commun. 251 (2005) 388–392.
[6] P.T. Diallo, P. Boutinaud, R. Mahiow, J.C. Cousseins, Red luminescence in Pr^{3+}-doped calcium titanates, Phys. Status Solidi A 160 (1997) 255–263.
[7] D. Peng, H. Sun, X. Wang, J. Zhang, M. Tang, X. Yao, Red emission in Pr doped $CaBi_4Ti_4O_{15}$ ferroelectric ceramics, Mater. Sci. Eng. B 176 (2011) 1513–1516.
[8] W. Tang, Y. Sun, M. Yu, X. Liu, Y. Yin, B. Yang, L. Zheng, F. Qin, Z. Zhanga, W. Cao, White-light-emitting properties of $SrTiO_3$:Pr^{3+} nanoparticles, RSC Adv. 5 (2015) 27491–27495.
[9] C. De Mello Donegá, Meijerink, G. Blasse, Non-radiative relaxation processes of the Pr^{3+} ion in solids, J. Phys. Chem. Solids 56 (1995) 673–685.
[10] E.G. Reut, A.I. Ryskin, Virtual recharge: mechanism of radiationless transition in scheelite and fergusonite type crystals doped with rare-earth ions, Phys. Status Solidi A 17 (1973) 47–57.
[11] G. Blasse, Vibronic transitions in rare earth spectroscopy, Int. Rev. Phys. Chem. 11

(1992) 71–100.
[12] E. Pinel, P. Boutinaud, R. Mahiou, What makes the luminescence of Pr^{3+} different in $CaTiO_3$ and $CaZrO_3$? J. Alloy. Compd. 380 (2004) 225–229.
[13] Y. Jin, Y. Hu, L. Chen, X. Wang, G. Ju, Z. Mou, Luminescence properties of dual-emission (uv/visible) long afterglow phosphor $SrZrO_3$: Pr^{3+}, J. Am. Ceram. Soc. 96 (2013) 3821–3827.
[14] S. Sakka, Handbook of Sol-Gel Science and Technology, Processing, Characterization and Applications, Kluwer Academic Publishers, New York, 2005.
[15] A.Z. Simoes, C. Quinelato, A. Ries, B.D. Stojanovic, E. Longo, J.A. Varela, Preparation of lanthanum doped $Bi_4Ti_3O_{12}$ ceramics by the polymeric precursor method, Mater. Chem. Phys. 98 (2006) 481–485.
[16] H. Guo, Y. Qiao, Preparation, structural and photoluminescent properties of CeO_2:Eu^{3+} films derived by Pechini sol–gel process, Appl. Surf. Sci. 254 (2008) 1961–1965.
[17] A. Ikesue, I. Furusato, K. Kamata, Fabrication of polycrystalline, transparent YAG ceramics by a solid-state reaction method, J. Am. Ceram. Soc. 78 (1995) 225–228.
[18] M. Ferrari, L. Lutterotti, Method for the simultaneous determination of anisotropic residual stresses and texture by x-ray diffraction, J. Appl. Phys. 76 (1994) 7246–7255.
[19] L. Weston, A. Janotti, X.Y. Cui, B. Himmetoglu, C. Stampfl, C.G. Van de Walle, Structural and electronic properties of $SrZrO_3$ and $Sr(Ti,Zr)O_3$ alloys, Phys. Rev. B 92 (2015) 085201.
[20] B.J. Kennedy, C.J. Howard, B.C. Chakoumakos, High-temperature phase transitions in $SrZrO_3$, Phys. Rev. B 59 (1999) 4023.
[21] H. Okamoto, K. Kasuga, I. Hara, Yoshinori Kubota, Visible–NIR tunable Pr^{3+}-doped fiber laser pumped by a GaN laser diode, Opt. Express 17 (2009) 20227–20232.
[22] A. Lazarowska, S. Mahlik, M. Krosnicki, M. Grinberg, M. Malinowski, Pressure-induced phase transition in $LiLuF_4$:Pr^{3+} investigated by an optical technique, J. Phys. Condens. Matter 24 (2012) 115502.
[23] A.J.H. Macke, Investigations on the luminescence of titanium-activated stannates and zirconates, J. Solid State Chem. 18 (1976) 337–346.
[24] L.G.J. de Haart, A.J. de Vries, G. Blasse, On the photoluminescence of semiconducting titanates applied in photoelectrochemical cells, J. Solid State Chem. 59 (1985) 291–300.
[25] P. Dorenbos, Modeling the chemical shift of lanthanide 4f electron binding energies, Phys. Rev. B 85 (2012) 165107.
[26] P. Dorenbos, A review on how lanthanide impurity levels change with chemistry and structure of inorganic compounds, ECS J. Solid State Sci. Technol. 2 (2013) R3001–R3011.
[27] E.G. Rogers, P. Dorenbos, Vacuum energy referred $Ti^{3+/4+}$ donor/acceptor states in insulating and semiconducting inorganic compounds, J. Lumin. 153 (2014) 40–45.
[28] P. Dorenbos, The electronic structure of lanthanide doped compounds with 3d, 4d, 5d, or 6d conduction band states, J. Lumin. 151 (2014) 224–228.
[29] P. Boutinaud, E. Pinel, M. Oubaha, R. Mahiou, E. Cavalli, M. Bettinelli, Making red emitting phosphors with Pr^{3+}, Opt. Mater. 28 (2013) 9–13.
[30] P. Boutinaud, R. Mahiou, E. Cavalli, M. Bettinelli, Luminescence properties of Pr^{3+} in titanates and vanadates: towards a criterion to predict $^3P_0$ emission quenching, Chem. Phys. Lett. 418 (2006) 185–188.
[31] V.M. Longo, L.S. Cavalcante, R. Erlo, V.R. Mastelaro, A.T. de Figueiredo, J.R. Sambrano, S. de Lázaro, A.Z. Freitas, L. Gomes, N.D. Vieira Jr., J.A. Varela, E. Longo, Strong violet–blue light photoluminescence emission at room temperature in $SrZrO_3$: joint experimental and theoretical study, Acta Mater. 56 (2008) 2191–2202.
[32] C. Guo, X. Ding, Y. Xu, Luminescent properties of Eu^{3+}-doped $BaLn_2ZnO_5$ (Ln=La, Gd, and Y) phosphors by the sol–gel method, J. Am. Ceram. Soc. 93 (2010) 1708–1713.